Vertical-Cavity Silicon-Integrated Laser with In-Plane Waveguide Emission at 850 nm

N.B. When citing this work, cite the original published paper.

(article starts on next page)

Abstract A continuous-wave electrically-pumped short-wavelength hybrid vertical-cavity silicon-integrated laser (VCSIL) with in-plane emission into a silicon nitride (SiN) waveguide is experimentally demonstrated. The coupling from the vertical cavity into the in-plane SiN waveguide is achieved by a weak grating on the SiN waveguide placed inside the cavity. The grating provides coupling, sets the polarization of the lasing output, and provides transverse mode control. A 5 μm oxide-aperture diameter device with a threshold current of 1.1 mA produces 73 μW single-sided waveguide-coupled optical output power at 2.6 mA bias current at a wavelength of 856 nm and a side-mode suppression ratio (SMSR) of 29 dB.

250 μm

ORIGINAL PAPER
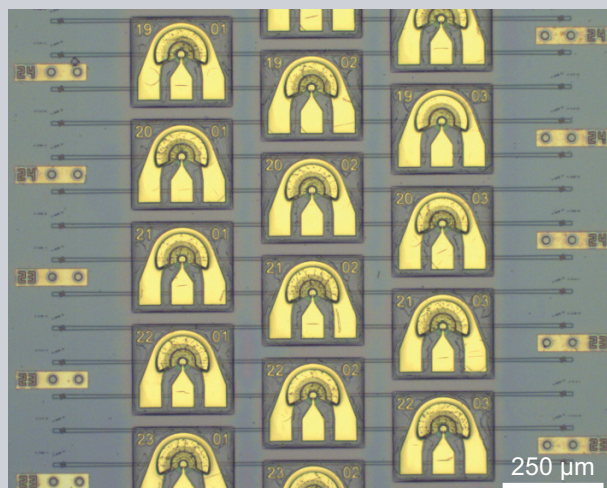
Vertical-cavity silicon-integrated laser with in-plane waveguide emission at 850 nm

Sulakshna Kumari[1,2,*] **Emanuel P. Haglund**[3] **, Johan S. Gustavsson**[3]**, Anders Larsson**[3]**, Gunther Roelkens**[1,2]**, and Roel G. Baets**[1,2]

1. Introduction

Over the past decades, considerable efforts have been invested in research, development and industrialization of silicon (Si) photonics. As a result Si photonics has emerged as a mature technological platform for optical datacom and telecom applications at 1310 and 1550 nm. However for applications requiring shorter wavelengths, Si cannot be used due to the absorption in Si below 1.1 μm. Instead silicon nitride (SiN) can be used as a substitute of Si, providing similar circuit compactness, resulting from the relatively high refractive index contrast between SiN (n $\approx$ 2) and silicon dioxide (SiO$_2$, n $\approx$ 1.5), and can be manufactured using the same complementary metal oxide semiconductor (CMOS) fabrication infrastructure as Si [1]. SiN has particular relevance for life science applications, because of the therapeutic window at visible and very near-IR wavelengths for biological media, where the photo-damage of cells is minimal and water absorption is negligible.

While there has been a rapid development of different optical components such as low-loss waveguides and spectrometers [1–3] on the SiN platform, the realization of integrated light sources on SiN is still a major challenge. So far, the SiN photonic integrated circuits have been demonstrated with external light sources. Hence, an integrated

laser source in such densely integrated circuits would provide immense potential for applications such as medical point-of-care devices, bodily implants for monitoring of glucose levels, and sensing devices integrated in smartphones. Various approaches to integrate III-V light sources into Si waveguides have been demonstrated, for example by direct growth of III-V on Si [4], die-to-wafer and wafer-to-wafer bonding [5,6], flip-chip integration [7–11] and transfer printing [12]. A review of different integration approaches has recently been published in [13].

The most power efficient low-current/low-power semiconductor laser available today is the vertical-cavity surface-emitting laser (VCSEL) with demonstrated power conversion efficiencies exceeding 60% [14]. Such a light source could offer a compact, and inexpensive wafer scale solution with low power consumption. While VCSELs were developed mainly for data communication application, they have also gained attraction in applications such as optical sensing, spectroscopy, atomic clocks [15], etc. Therefore, VCSELs are of great interest to be integrated into SiN waveguide circuits. For several of these applications, there is a need for a single mode, polarization stable laser source.

One of the hybrid integration approaches is to flip chip a VCSEL onto a grating coupler on a Si/SiN photonic integrated circuit (PIC). There have been reports on flip-chipped

[1] Photonics Research Group, Ghent University-imec, Technologiepark-Zwijnaarde 15, 9052 Ghent, Belgium
[2] Center for Nano- and Biophotonics, Ghent University, 9000 Ghent, Belgium
[3] Photonics Laboratory, Department of Microtechnology and Nanoscience, Chalmers University of Technology, SE-41296 Gteborg, Sweden
[*] Corresponding author: e-mail: sulakshna.kumari@ugent.be

VCSELs on a Si grating coupler to couple the vertical emission from a VCSEL to an in-plane Si waveguide using a perfectly vertical grating coupler [7, 8] and using an angled grating coupler [9, 10]. Recently, a hybrid vertical-cavity laser (VCL) with a single-mode output using a silicon high contrast grating (HCG) was demonstrated using flip-chip integration [11]. In these hybrid structures the standing wave optical field extends over both the III-V material, containing the gain region and a single DBR, and the Si-based structure, containing the HCG. Despite of having the advantage of pretesting the III-V components prior to the assembly with the Si/SiN PIC, flip-chip technique suffers from not being wafer scale process and from requiring accurate and time-consuming alignment of individual devices. Another integration approach is heterogeneous integration, which has the advantage of being a wafer scale process. Heterogeneously integrated optically pumped lasers with polarization independent 2D HCG [16], and polarization dependent 1D HCG providing coupling to in-plane Si waveguides [17] have also been demonstrated.

Our approach is to bond an epitaxial half-VCSEL structure onto a CMOS-compatible dielectric distributed Bragg reflector (DBR) on a Si substrate, forming a hybrid cavity [18]. By placing a waveguide with a weak diffraction grating inside the cavity, between the dielectric DBR and the half-VCSEL, it is possible to tap off light into in-plane waveguide [19]. We took the first step towards the realization of such a device with the demonstration of a hybrid-cavity VCSEL on silicon, but without the intra-cavity waveguide [18]. These VCSELs were surface emitting and thus acted as a stepping-stone in the development of the integration technique. Further, we numerically investigated the possibility of coupling the output of the hybrid vertical-cavity laser to an in-plane SiN waveguide using an intra-cavity diffraction grating [20]. As this design was not surface emitting, we referred to it as a vertical-cavity silicon-integrated laser (VCSIL). We showed that a design with high coupling efficiency and polarization selection is feasible.

In this paper, we report on a single-mode, polarization-stable, short-wavelength VCSIL heterogeneously integrated on a SiN PIC that couples into a SiN waveguide based on the design presented in [20]. To the best of the authors' knowledge, this is the first demonstration of a heterogeneously-integrated electrically-pumped VCSIL with emission into a SiN-based waveguide.

2. Concept and Design

As can be seen in Figure 1, the VCSIL structure comprises two distinct parts referred to as the top half-structure and the bottom half-structure. The top half-structure is a GaAs-based half-VCSEL identical to the one used in [18, 21], consisting of a top p-doped $Al_{0.12}Ga_{0.88}As/Al_{0.90}Ga_{0.10}As$ DBR with 23 mirror pairs, a 1-λ-thick separate confinement heterostructure (SCH) containing five 4-nm-thick $In_{0.10}Ga_{0.90}As/Al_{0.37}Ga_{0.63}As$ quantum wells, and a 1-λ-thick n-doped $Al_{0.12}Ga_{0.88}As$ current spreading layer (CSL). A 30-nm-thick layer of $Al_{0.98}Ga_{0.02}As$ is included in the
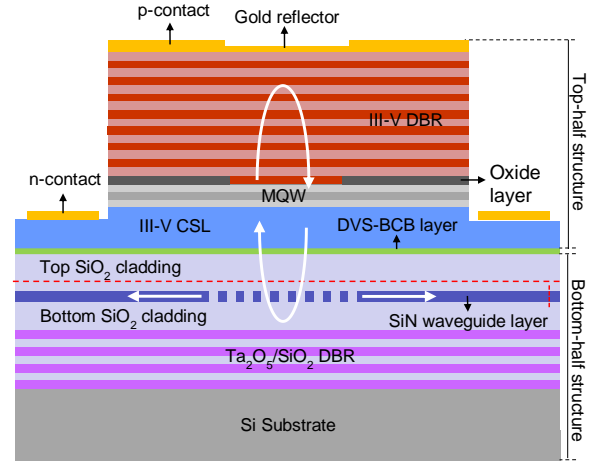

Figure 1 Schematic cross-section of the VCSIL with in-plane out-coupling into a SiN waveguide. The red dotted lines are the reference planes where reflection and single-sided coupling coefficient are calculated.

DBR mirror pair closest to the SCH, for the formation of an oxide aperture via selective oxidation. The top-half structure is covered by a 100 nm thick gold film to avoid surface emission, whereby the topmost GaAs layer thickness has been adjusted for phase matching to the gold. The bottom-half structure is a SiN-waveguide/dielectric-DBR combination on a Si substrate consisting of a weak diffraction grating etched in an intra-cavity SiN waveguide placed on top of a CMOS-compatible 20-pair Ta_2O_5/SiO_2 dielectric bottom DBR identical to the one used in [18, 21]. The top and bottom SiO_2 cladding layers prevent the waveguide mode to leak into the high index GaAs half-VCSEL and the high index dielectric DBR and Si substrate. A 50-nm-thick divinylsiloxane-bis-benzocyclobutene (DVS-BCB) adhesive bonding layer is used to attach the top half-structure to the bottom-half structure.

As the arrows in Figure 1 illustrate, light is amplified vertically between the III-V top DBR and the intra-cavity grating/dielectric bottom DBR combination, and a fraction of this light energy is coupled out into a SiN waveguide. The intra-cavity grating is designed in such a way that the combination of the grating and the DBR reflects most of the light and couples a small fraction of the light into the SiN waveguide. This is by design the dominant (useful) cavity loss. In principle the waveguide-coupled output power of the VCSIL can be similar to that of any other single-mode VCSEL with a similar thermal impedance. As compared to edge-emitting lasers one can expect that useful output powers of 100's of μW up to few mW can be reached at much lower bias current, but the maximum output power will be considerably lower than is the case for edge-emitting lasers, where it can reach tens to hundreds of mW.

To design such a grating, a 2D FDTD simulation was performed using a commercial simulator Lumerical on the bottom half-structure of the VCSIL [20]. A Gaussian beam with a width similar to the fundamental VCSIL mode was

launched from inside the top SiO$_2$ cladding layer (100 nm above the intra-cavity grating layer) perpendicular to the bottom half structure of the VCSIL. The fraction of incident optical power that is on one hand reflected by the grating/dielectric bottom DBR combination (reflection coefficient) and on the other hand coupled to the SiN waveguide (single-sided coupling coefficient) is calculated at the reference planes (red dotted lines in Figure 1). Note that the output coupling by the intra-cavity grating is bi-directional. Therefore, the coupling to each side of the in-plane waveguide is the same, with the single-sided coupling coefficient being the fraction of incident light being coupled into each waveguide. As discussed in [20], a GaAs VCSIL with aperture diameter > 4 μm is required to have a polarization selective intra-cavity grating/dielectric DBR combination with sufficient reflection and coupling of the fundamental transverse electric (TE) mode into the SiN waveguide. The TE mode is polarized along the intra-cavity grating lines, while the transverse magnetic (TM) mode is polarized across the grating lines.

To realize a device with the above-mentioned features, an oxide aperture diameter of 5 μm (corresponding to a 1/e^2 beam diameter of 4.7 μm) was chosen. For the surface-emitting hybrid devices demonstrated in [18], the gain peak was estimated to be at 852 nm, which resulted in superior room temperature performance of VCSELs operating at $\sim$ 855 nm [21]. Therefore, we chose to design VCSILs operating at 855 nm, as the III-V layer structure used in this work is identical to the one used in [21]. Figure 2 shows the simulated reflection and single-sided coupling coefficient for the intra-cavity grating/DBR combination as function of wavelength and polarization for a grating period of 530 nm and a 50% duty cycle (DC). At 855 nm, it can be seen in Figure 2(b) that the grating is designed to operate far from the center Bragg wavelength for coupling the vertically propagating light into the SiN waveguide. In particular the TE mode operates further away from the Bragg wavelength than the TM mode. This results in higher cavity losses for the TM mode, which can be used to prevent the TM mode from lasing, i.e. set the lasing polarization state of the VCSIL to TE.

An increment in the grating period redshifts the reflection and single-sided waveguide coupling spectrum for both TE and TM polarizations. Figure 3 shows the simulated reflection and single-sided coupling coefficient as function of the grating period at a resonance wavelength of 855 nm for the two polarizations. As can be seen from Figure 3(a), the intra-cavity grating favors lasing of the TE polarization for grating periods ranging from 520 - 550 nm, while also providing coupling into the SiN waveguide, see Figure 3(b). To estimate the optical cavity properties of the VCSIL, such as the cavity resonance wavelength, threshold gain and the slope efficiency, a 1D transfer matrix method (TMM) was used. The bottom dielectric DBR combination was replaced with an artificial interface having the wavelength dependent reflection and single-sided coupling coefficient obtained from the 2D FDTD simulations [20]. The cavity length of the VCSEL was adjusted to set the resonance wavelength of the cavity at 855 nm. For a top SiO$_2$ cladding thickness of
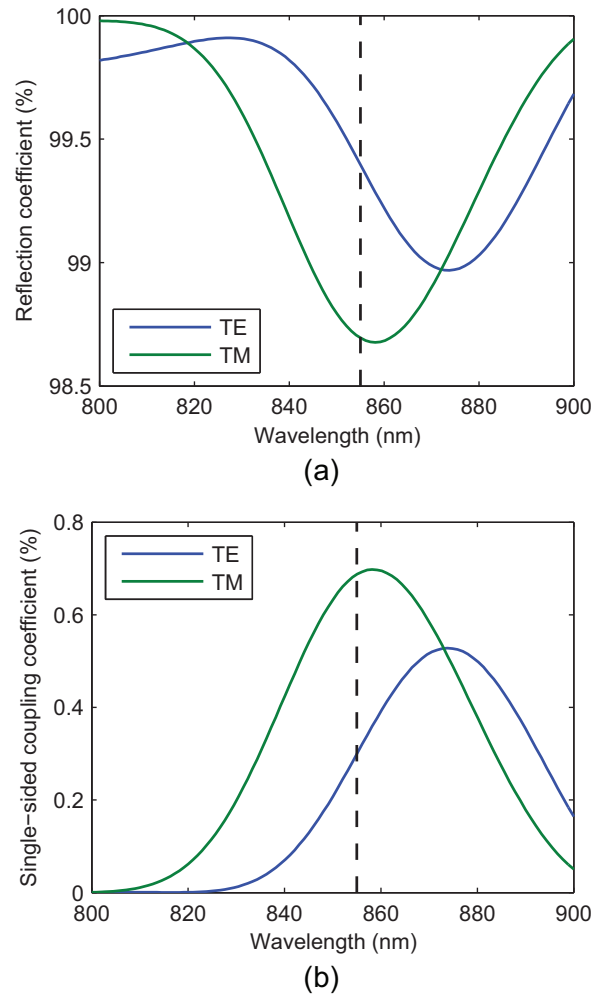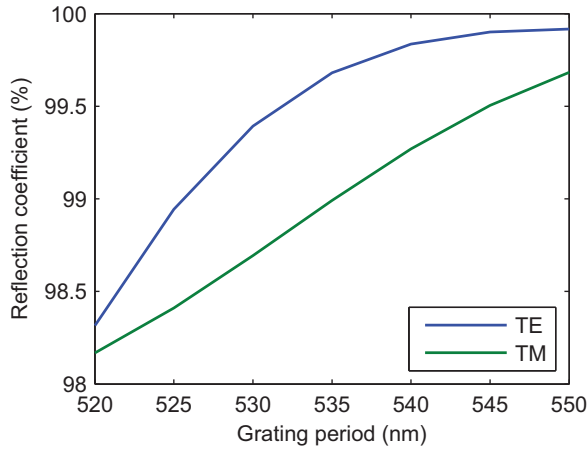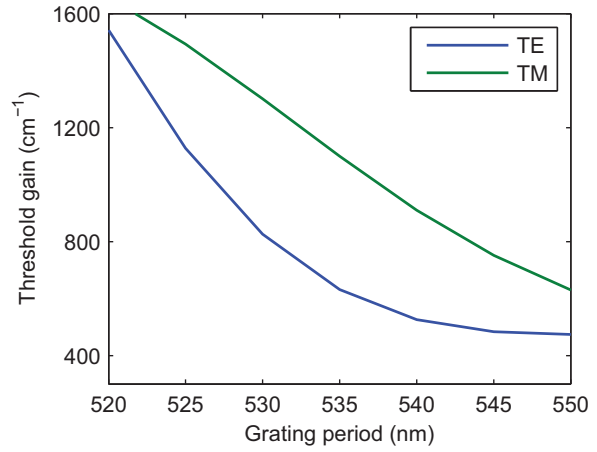

(a)

(b)

Figure 2 (a) Simulated reflection coefficient and (b) single-sided coupling coefficient of the bottom-half structure as a function of wavelength for TE and TM polarizations. (grating period = 530 nm, DC = 50%)

780 nm with DVS-BCB layer of 50 nm, this condition was achieved. The calculated threshold gain and single-sided slope efficiency (assuming an internal quantum efficiency of 85%) as function of the grating period at a resonance wavelength of 855 nm is shown in Figure 4. While the VCSILs with the smallest grating period provide high single-sided slope efficiency, the threshold gain required for lasing is large. Therefore the selection of an optimal intra-cavity grating period sets a trade-off between the threshold gain and single-sided slope efficiency. A threshold gain below 1000 cm^{-1} is typically required to ensure sub-mA threshold current (for GaAs-based VCSELs with an oxide aperture diameter < 10 μm). The higher threshold gain for the TM polarization, for grating periods between 520 nm and 550 nm, results in a relative dichroism much higher than the 1% required for a large polarization suppression ratio [22]. A change in the thickness of top SiO$_2$ cladding layer influences the optical cavity properties such as the cavity resonance wavelength, threshold gain and single-sided slope efficiency.
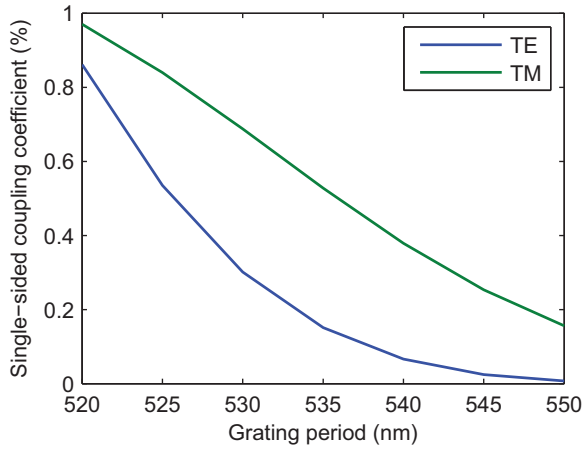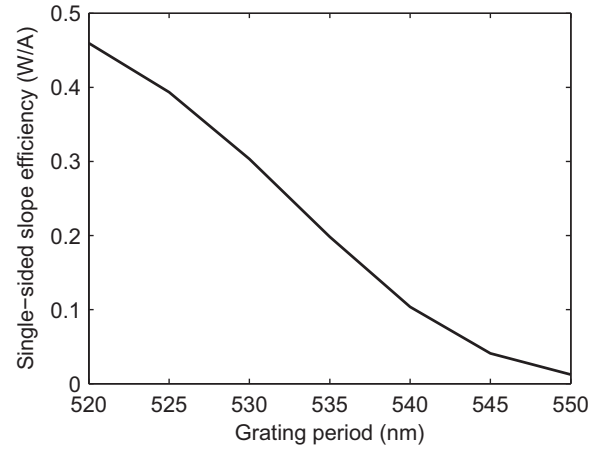
Figure 3 (a) Simulated reflection coefficient and (b) single-sided coupling coefficient of the bottom-half structure as a function of intra-cavity grating period for TE and TM polarizations at a resonance wavelength of 855 nm.

Figure 4 (a) Simulated threshold material gain in quantum wells (TE and TM polarization) and (b) single-sided slope efficiency (TE polarization) as a function of intra-cavity grating period at a resonance wavelength of 855 nm.

A brief discussion about the impact of the thickness of the top SiO_2 cladding layer is presented in [20]. For a structure with an optimal grating period, a ± 10 nm shift in thickness of top SiO_2 cladding layer corresponds to a resonance wavelength shift of maximum ± 1.3 nm while the threshold gain stays well below $1000\ cm^{-1}$ and the single-side slope efficiency stays well above 0.15 mW/mA [20].

Finally, fiber-to-chip grating couplers with 683 nm period and 50% DC were incorporated at the ends of the waveguide to be able to couple light from the SiN waveguide to an optical fiber. In contrast to the intra-cavity grating, the grating couplers have an etch depth of 300 nm and have a theoretical coupling efficiency to single mode fiber of -4.2 dB at 855 nm.

3. Device Fabrication

To add the SiN waveguide layer on top of the dielectric DBR used in [18], a 610 nm thick PECVD bottom SiO_2 cladding layer and a 300 nm thick low-frequency PECVD SiN waveguide layer was deposited at 270°C. The thickness of the deposited SiO_2 and SiN was accurately monitored using ellipsometry. Intra-cavity gratings with five different periods, varying from 525 - 545 nm, and three different DCs, varying from 45 - 55%, were defined in the SiN waveguide layer using electron-beam lithography. The intra-cavity grating was etched 30 nm using reactive ion etching (RIE) with a SF_6, CF_4 and H_2 mixture. Thereafter, the grating couplers and the interconnecting waveguides were defined, also using electron-beam lithography. This pattern was fully etched (300 nm), again using RIE with a SF_6, CF_4 and H_2 mixture. A 780 nm thick top PECVD SiO_2 cladding layer was finally deposited. The GaAs half-VCSEL epitaxial structure (4 x 12 mm die) was bonded on top of the patterned

structure using DVS-BCB adhesive bonding using a similar process as in [5], followed by the removal of the GaAs substrate. A DVS-BCB:mesitylene (1:3) solution spin coated at 3000 rpm on the top PECVD SiO_2 cladding layer and an applied bonding pressure of 300 kPa results in a 50 nm thick DVS-BCB bonding layer (after curing the DVS-BCB at 280°C), while also planarizing the top oxide cladding surface to within ± 5 nm. The thickness of the BCB layer can be controlled to within ± 10 nm. VCSIL devices were then fabricated using a similar process as in [18]. To accurately align the VCSILs on top of the intra-cavity gratings, direct laser writing was used to pattern the top contact rings and the III-V mesas. The direct laser writing technology has a throughput of 100 mm^2/min with 0.7 μm resolution and 200 nm alignment accuracy. For large scale fabrication it can be exchanged with a stepper. Any remaining AlGaAs material on top of the waveguides was removed outside the device structure to reduce the possibility of power leakage from the waveguide to the higher refractive index AlGaAs material. Finally, the surface-emission was suppressed by electron beam deposition of a 100 nm gold film on top of the III-V mesas. Figure 5 shows microscope images of fully fabricated VCSILs on top of intra-cavity gratings and waveguide structures.

4. Measurements

To evaluate the properties of the VCSIL cavity, the surface emission was studied prior to the deposition of the surface gold layer. At this stage the structure with the weakest single-sided coupling coefficient (using a grating period of 545 nm) shows best lasing behaviour whereas the grating with the strongest single-sided coupling coefficient (520 nm grating period) shows almost no lasing behaviour due to overall high cavity losses. Figure 6(a) shows the polarization-resolved light-current-voltage (LIV) characteristics at 25°C of a device with an intra-cavity grating period of 545 nm and 50% DC, measured from the surface using a free-space polarizer and a large area Si photodetector. The measurement result shows that the cavity only supports lasing in the TE polarization, which is consistent with the simulations in Figure 3. The surface-emitted spectrum for the same device at a bias current of 2.5 mA is shown in Figure 6(b). The spectrum shows near single mode operation with a side-mode suppression ratio (SMSR) of 30.8 dB and a peak wavelength of 856.3 nm. This indicates that the cavity is mode selective enough to achieve near single mode emission. Without the gold layer on top of the surface to suppress surface emission, the waveguide-coupled power was weak due to the dominant cavity loss from the top surface emission. With this gold layer on the surface aperture, the waveguide coupled output from the VCSIL was coupled into a bare OM4 multi-mode fiber by a TE grating coupler (GC) with peak coupling efficiency near 855 nm. To be able to estimate the actual optical power coupled into the SiN waveguide from fiber coupled measurements, grating couplers were arranged in a back-to-back configuration. The coupling loss was determined from the measured insertion
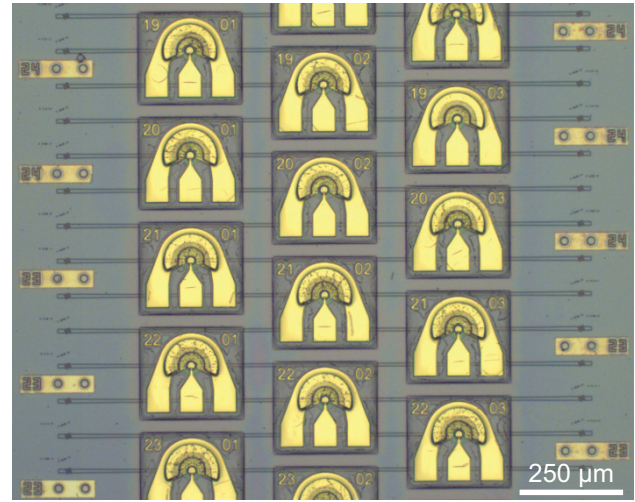
(a)
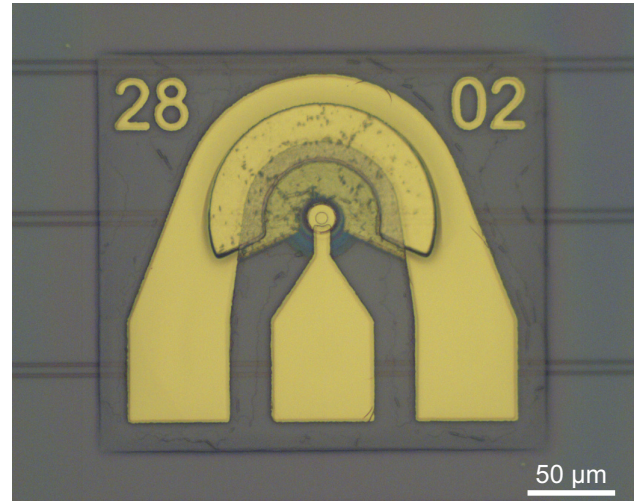
(b)

Figure 5 Optical micrographs of (a) an array of fully processed VCSILs and (b) a single VCSIL.

loss of two such back-to-back connected couplers, which also included the waveguide loss of the SiN waveguide in between. The waveguide has a width of 5.5 μm throughout the $\sim$ 1.6 mm length. Hence the waveguide loss was considered to be negligible. The coupling loss for each grating coupler was measured to be -5.75 dB for coupling to a multimode fiber with core size of 62.5 μm at a wavelength of 855 nm.

The single-sided on-chip continuous LIV characteristics of VCSILs with five intra-cavity grating periods ranging from 525 to 545 nm and with 55% DC were then measured at 25°C using a fiber-coupled power meter, as shown in Figure 7(a), whereby the GC loss was taken into account. The variation of threshold current with intra-cavity grating period is expected to follow the variation of the threshold gain predicted by the simulations (Figure 4(a)). However, the influence of the intra-cavity grating period on thresh-
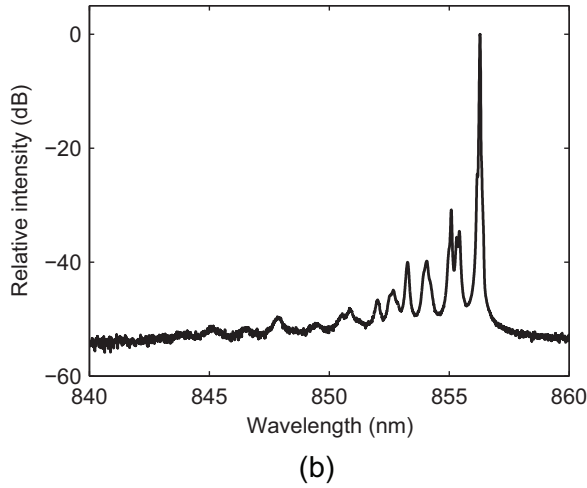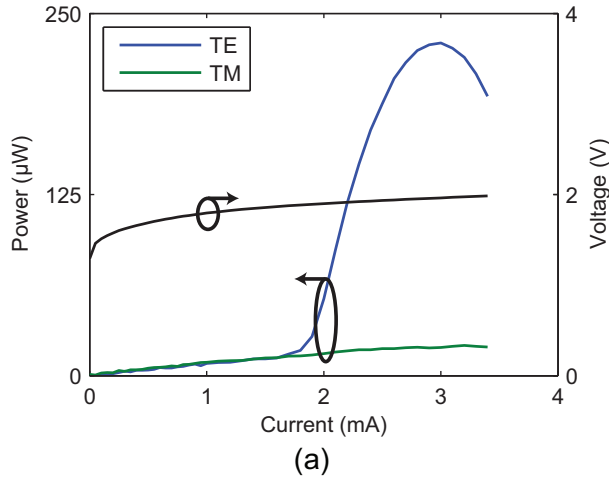
(a)

(b)

Figure 6 (a) Polarization-resolved surface-emitted light-current-voltage characteristics for a 5 μm oxide-aperture diameter VCSIL with 545 nm intra-cavity grating period and 50% DC (prior to gold deposition on surface). (b) Surface emitted spectrum for the same device operated at 2.5 mA.

(a)

(b)

Figure 7 (a) Waveguide-coupled light-current-voltage characteristics for 5 μm oxide-aperture diameter VCSILs with intra-cavity grating periods (GPs) ranging from 525 - 545 nm (after gold deposition on surface). (b) Spectrum for the 525 nm device operated at 2.5 mA.

old current is not as strong as numerically estimated in Figure 4(a). This indicates that there are unexpected dominant losses in the cavity due to surface roughness, material loss, etc. From Figure 7(a), we see that the slope efficiency trend is in agreement with the simulation in Figure 4(b), in terms of the reduction of the slope efficiency with increased intra-cavity grating period. There is a clear difference in the maximum output power that is coupled into the SiN waveguides for the different intra-cavity grating periods. A VCSIL with the smallest grating period of 525 nm exhibits a threshold current of 1.13 mA providing maximum single-sided waveguide-coupled output power of 73 μW at 2.6 mA bias current. The single-sided slope efficiency and the differential resistance for this device is 0.085 W/A and 78 Ω, respectively. Compared to the simulated single-sided slope efficiency in Figure 4(b), the experimental slope efficiency is somewhat lower, which could be due to the unexpected dominant cavity losses. The on-chip spectrum for a VCSIL
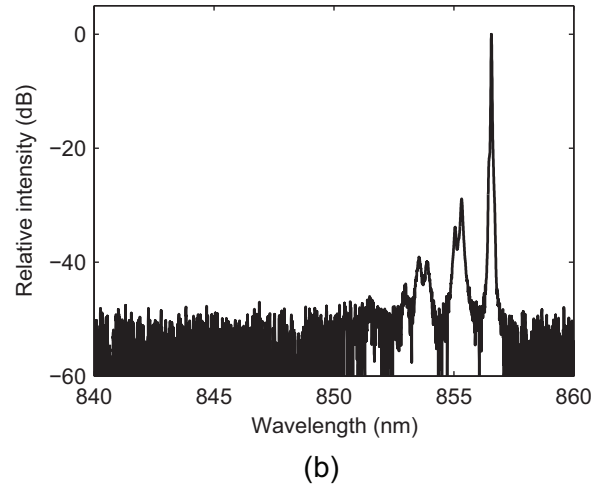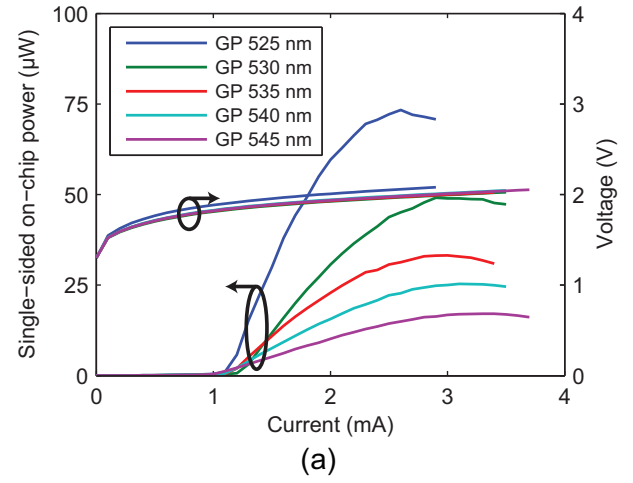
with intra-cavity grating period 525 nm, at bias current of 2.5 mA is shown in Figure 7(b). The SMSR is 28.9 dB, while the peak wavelength is at 856.6 nm.

As can be seen from the spectra in Figure 6(b) and Figure 7(b), the demonstrated VCSIL has better transverse mode control than ordinary oxide-confined VCSELs with the same aperture size [23], both before and after deposition of gold on the surface aperture. This can be attributed to the fact that the higher order transverse modes contain spatial frequency components with larger off-normal angles than the fundamental mode. These couple more efficiently to the waveguide through the grating, thereby leading to an increase of the threshold gain. This was also the effect that required the size of the oxide aperture to be larger than 4 μm for sufficient grating/DBR reflection in [20]. Since the gain is clamped at the threshold gain of the fundamental mode, a good transverse mode control is expected from the grating.
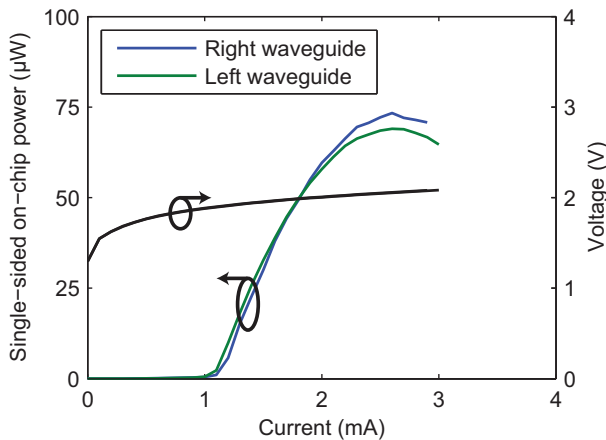
Figure 8 Measured light-current-voltage characteristics where the power has been measured from both grating couplers for a VCSIL with 525 nm intra-cavity grating period and 55% DC.

The thermal impedance of the VCSIL was deduced by tracking the red shift of the fundamental mode as function of stage temperature and dissipated power [24]. At 25°C the fundamental mode redshifts with 0.052 nm/K, while it redshifts with dissipated power by 0.61 nm/mW giving a thermal impedance of 11.8 K/mW, which is similar to the 10.7 K/mW of our previous silicon-integrated surface-emitting device with the same aperture diameter [23]. The thermal impedance is ~ 4 times higher than ordinary GaAs-based oxide-confined VCSELs [25] and explains the early onset of thermal rollover in both these cases.

Finally, the coupling symmetry was studied. As can be seen in Figure 8, an equal amount of power is tapped off into both of the two connected waveguides. This indicates that the VCSIL aperture is well aligned with the intra-cavity grating.

5. Conclusion

In summary, we have demonstrated a heterogeneously integrated continuous-wave electrically-pumped vertical-cavity Si-integrated laser (VCSIL) with laser output coupled into SiN waveguides using a shallow etched intra-cavity SiN grating. The intra-cavity grating provides the advantage of setting the polarization of the output coupled into the SiN waveguide together with transverse mode control. A VCSIL with a 5 μm oxide aperture diameter has a threshold current of 1.13 mA and produces a maximum single-sided waveguide coupled output power of 73 μW at $\sim$ 856 nm. The slope efficiency and the thermal impedance of the corresponding device is 0.085 W/A and 11.8 K/mW, respectively. The performance of the present VCSILs is inferior to the VCSELs presented in [21], in terms of threshold current and output power, which is to a large extent is limited by the high thermal impedance due to the dielectric DBR and unexpected cavity losses attributed to surface roughness and material absorption. With the identification of the origin of

the unexpected cavity losses in the VCSIL cavity and by lowering the thermal impedance by using integrated metallic heat spreaders or thermal shunts, significant performance improvements are expected. The presented device can be extended to cover other wavelength ranges as well.

Key words: On-chip laser source, silicon photonics, intra-cavity grating, vertical-cavity silicon-integrated laser, semiconductor lasers.

References

[1] A. Z. Subramanian, E. Ryckeboer, A. Dhakal, F. Peyskens, A. Malik, B. Kuyken, H. Zhao, S. Pathak, A. Ruocco, A. D. Groote, P. Wuytens, D. Martens, F. Leo, W. Xie, U. D. Dave, M. Muneeb, P. V. Dorpe, J. V. Campenhout, W. Bogaerts, P. Bienstman, N. L. Thomas, D. Van. Thourhout, Z. Hens, G. Roelkens, and R. Baets, Photonics Research, **3**, pp. B47-BB59, (2015).
[2] A. Z. Subramanian, P. Neutens, A. Dhakal, R. Jansen, T. Claes, X. Rottenberg, F. Peyskens, S. Selvaraja, P. Helin, B. DuBois, K. Leyssens, S. Severi, P. Deshpande, R. Baets, and P. V. Dorpe, IEEE Photon. J., **5**, p. 2202809, (2013).
[3] D. Martens, A. Z. Subramanian, S. Pathak, M. Vanslembrouck, P. Bienstman, W. Bogaerts, and R. G. Baets, IEEE Photonics Technol. Lett. **27**, pp. 137-140, (2015).
[4] Z. Wang, B. Tian, M. Pantouvaki, W. Guo, P. Absil, J. V. Campenhout, C. Merckling, D. Van. Thourhout, Nat. Photon., **9**, pp. 837-842, (2015).
[5] S. Keyvaninia, M. Muneeb, S. Stankovic, P. J. Van Veldhoven, D. Van Thourhout, and G. Roelkens, Opt. Mater. Express, **3**, pp. 35-46, (2013).
[6] H. Li, X. Ma, B. Cui, Y. Wang, C. Zhang, J. Zhao, Z. Zhang, C. Tang, and E. Li, Optica, **4**, p. 692, (2017).
[7] Y. Wang, S. S. Djordjecvic, J. Yao, J. E. Cunningham, X. Zheng, A. V. Krishnamoorthy, M. Muller, M-C. Amann, R. Bojko, N. A. F. Jaeger and L. Chrostowski, Proceedings of IEEE Optical Interconnects Conference (OI), IEEE, pp. 122-123, (2015).
[8] Y. Yang, G. Djogo, M. Haque, P. R. Herman, J. K. S. Poon, Opt. Express **25**, pp. 5758–5771, (2017).
[9] K. S. Kaur, A. Z. Subramanian, P. Cardile, R. Verplancke, J. Van Kerrebrouck, S. Spiga, R. Meyer, J. Bauwelinck, R. Baets, G. V. Steenberge, Opt. Express, **23**, pp. 28264-28270, (2015).
[10] H. Lu, J. S. Lee, Y. Zhao, C. Scarcella, P. Cardile, A. Daly, M. Ortsiefer, L. Carroll, and P. O'Brien, Opt. Express, **24**, pp. 16258-16266, (2016).
[11] J. Ferrara, W. Yang, L. Zhu, P. Qiao, and C. J. Chang-Hasnain, Opt. Express **23**, pp. 2512-2523, (2015).
[12] A. D. Groote, P. Cardile, A. Subramanian, A. Fecioru, C. Bower, D. Delbeke, R. Baets, G. Roelkens, Opt. Express, **24**, pp. 13754-13762, (2016).

[13] Z. Wang, A. Abbasi, U. D. Dave, A. De Groote, S. Kumari, B. Kunert, C. Merckling , M. Pantouvaki, Y. Shi, B. Tian, K. Van Gasse, J. Verbist, R. Wang, W. Xie, J. Zhang, Y. Zhu, J. Bauwelinck, X. Yin, Z. Hens, J. Van Campenhout, B. Kuyken, R. Baets, G. Morthier, D. Van Thourhout, G. Roelkens, Laser Photon. Rev., **11**, pp. 1700063, (2017).

[14] K. Takaki, N. Iwa, K. Hiraiwa, S. Imai, H. Shimizu, T. Kageyama, Y. Kawakita, N. Tsukiji, and A. Kasukawa, Proc. IEEE Int. Semicond. Laser Conf., Paper no. PDP1., (2008).

[15] D. K. Serkland, G. M. Peake, K. M. Geib, R. Lutwak, R. M. Garvey, M. Varghese, and M. Mescher, Proceedings of SPIE, **6132**, pp. 613208-111, (2006).

[16] Y. Tsunemi, N. Yokota, S. Majima, K. Ikeda, T. Katayama, and H. Kawaguchi, Opt. Express, **21**, pp. 28685-28692, (2013).

[17] G. C. Park, W. Xue, A. Taghizadeh, E. Semenova, K. Yvind, J. Mrk, and I-S. Chung, Laser Photon. Rev., **9**, pp. L11-L15, (2015).

[18] E. P. Haglund , S. Kumari, P. Westbergh, J. S. Gustavsson, R. G. Baets, G. Roelkens, and A. Larsson, Opt. Express, **23**, pp. 33634-33640, (2015).

[19] D. A. Louderback, G. W. Pickrell, H. C. Lin, M. A. Fish, J. J. Hindi and P. S. Guilfoyle, Electron. Lett., **40**, pp. 1064-1065, (2004).

[20] S. Kumari, J. Gustavsson, E. P. Haglund, J. Bengtsson, A. Larsson, G. Roelkens, and R. Baets, IEEE Photon. J. **9**, p. 1504109, (2017).

[21] E. P. Haglund, S. Kumari, E. Haglund, J. S. Gustavsson, R. G. Baets, G. Roelkens, and A. Larsson, IEEE J. Select. Top. Quantum Electron., **23**, pp. 1700109, (2017).

[22] P. Debernardi, H. J. Unold, J. Maehnss, R. Michalzik, G. P. Bava, and K. J. Ebeling, IEEE J. Select. Top. Quantum Electron., **9**, pp. 1394-1404, (2003).

[23] E. P. Haglund, S. Kumari, P. Westbergh, J. S. Gustavsson, R. G. Baets, G. Roelkens, and A. Larsson, IEEE Photonics Technol. Lett., **28**, pp. 856859, (2016).

[24] W. Nakwaski, Opt. Quantum Electron., **28**, pp. 335352, (1996).

[25] P. P. Baveja, B. Kögel, P. Westbergh, J. S. Gustavsson, Å. Haglund, D. N. Maywar, G. P. Agrawal, and A. Larsson, IEEE J. Quantum Electron., **48**, pp. 1726, (2012).